The Effect of Hip Assistance Levels on Human Energetic Cost Using Robotic Hip Exoskeletons

Inseung Kang, Hsiang Hsu, and Aaron Young, *Member, IEEE*

***Abstract*—In order for the lower limb exoskeletons to realize their considerable potential, a greater understanding of optimal assistive performance is required. While others have shown positive results, the fundamental question of how the exoskeleton interacts with the human remains unknown. Understanding the optimal assistance magnitude is not simply relevant for control, it is a critical knowledge for exoskeleton designers. An accurate understanding of assistance levels will enable the designers to minimize exoskeleton mass and improve the performance by avoiding excessive actuators and drivetrains. We explored the relationship between the assistance magnitude and the energetic cost benefits by using a series elastic actuator driven powered hip exoskeleton. The exoskeleton controller mimics a human biological hip moment to provide the assistance during the gait cycle. Ten able-bodied subjects walked using the exoskeleton with different magnitudes of assistance in both hip flexion and extension. Generally, the resulting metabolic cost across different assistance conditions showed a U-shape trend which was consistent across all subjects ($p < 0.01$). The interpreted optimal assistance point through the quadratic fit resulted in a 6% metabolic cost reduction with respect to the no-assistance condition. The study validated that simply increasing the assistance level did not yield higher energetic return.**

***Index Terms*—Wearable robots, human performance augmentation, robotic exoskeleton, energetic cost, hip orthosis.**

I. Introduction

LOWER limb exoskeleton technology has advanced greatly in the recent years and showed significant value in different applications [1]–[3]. Most of these technologies can be broken down into three main categories: industry settings, military purposes, and healthcare environments [1]. Several exoskeletons have been developed for industry usages where factory workers wear an exoskeleton suit to enhance physical strength to alleviate work load when lifting heavy weights [4], [5]. Another usage of exoskeleton technology is in the military settings where an exoskeleton can assist a soldier in safely and efficiently carry a heavy load over long such as when a solider would carry heavy loads while walking over long distances [6], [7]. Lastly, exoskeletons are used in the healthcare environment as an assistive device for patients with disabilities such as stroke, spinal cord injury, and muscular dystrophy [8]–[10]. Patients using these technologies in healthcare settings can not only regain mobility options, but also potentially benefit from long-term rehabilitation strategies [11]. Some of these exoskeletons such as Indego [8], Rewalk [9], and Ekso [12] have been commercialized in the market for medical applications. These devices frequently feature actuators at every joint, which makes the devices heavy and challenging to control. While these devices may benefit patients with a complete lower limb paralysis, their benefit for less impaired subjects remains less clear [13].

To accommodate such limitations of full body exoskeletons, several research and industry groups started to develop single joint actuated exoskeletons that are more suitable to both able-bodied humans and patients with partial gait disability (i.e., stroke survivors) [14]–[17]. Often these exoskeletons have targeted the ankle due to the joint providing a high mechanical power during walking. Several ankle exoskeletons were able to show positive results in achieving higher metabolic benefits when walking with assistance at the ankle joint [14], [18]. Recent literature studies have shown that the hip joint also plays a leading role in providing high mechanical power, up to 45%, during walking [19]. The ankle joint efficiently utilizes the Achilles tendon unit in storing the mechanical energy to perform positive joint power. However, due to different muscle characteristics and the lack of efficient elastic storage elements, the hip joint requires higher energetic cost for similar mechanical joint power [20]. Therefore, the hip joint represents an important area of exploration for engineers trying to increase human metabolic performance. Some of the hip exoskeletons that have been developed have shown positive outcomes [17], [21]–[25]. These exoskeletons are either autonomous with relatively low assistance levels or tethered to off board actuators to provide high magnitudes of assistance. Regardless, the majority of these devices have the same goal of achieving the best metabolic cost reduction. However, there is still a gap in understanding more in-depth relationships between energetic benefits and assistance levels.

The three key parameters that may contribute to the exoskeleton controller are onset timing, assistance duration, and assistance magnitude. Utilizing the assistance duration from the literature study [26], our previous work optimized the assistance onset timing for hip flexion and extension to achieve best metabolic cost reduction [27]. However, as the study provided a fixed magnitude of torque applied at the hip joint, it did not capture the effect of assistance magnitude in respect to the metabolic cost benefits. Thus, an extended study was required

Manuscript received July 18, 2018; accepted December 14, 2018. Date of publication January 4, 2019; date of current version January 16, 2019. This letter was recommended for publication by Associate Editor R. V. Patel and Editor A. Young upon evaluation of the reviewers' comments. This work was supported in part by the Georgia Tech Research Institute (GTRI) IRAD funding, in part by the Institute for Robotics and Intelligent Machines (IRIM) Seed Grant at Georgia Tech, and in part by the NSF NRI Award #1830215. *(Corresponding author: Inseung Kang.)*

The authors are with the Woodruff School of Mechanical Engineering, Georgia Institute of Technology, Atlanta, GA 30332 USA (e-mail: ikang7@gatech.edu; hhsu24@gatech.edu; aaron.young@me.gatech.edu).

This letter has supplementary downloadable multimedia material available at http://ieeexplore.ieee.org, provided by the author. This includes a video file, which includes three parts about the powered hip exoskeleton device. This material is 41.1 MB in size.

Digital Object Identifier 10.1109/LRA.2019.2890896

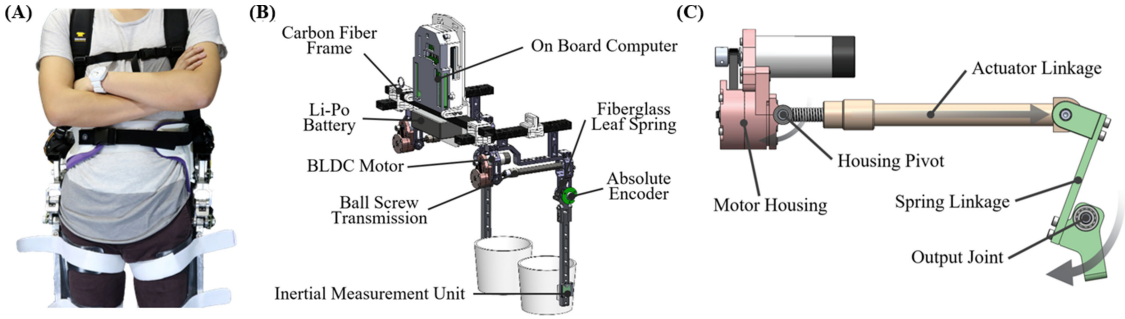

Fig. 1. Powered bilateral hip exoskeleton design. (A) The orthotic thigh shells, pelvic band, and shoulder straps can be adjusted to accommodate different body sizes. (B) Exoskeleton device consists of multiple sensors and actuators. (C) The brushless DC motor drives a timing belt pulley to extend and retract the ball screw transmission (orange) where the motor housing (red) pivots around the hinge to create torque around the output hip joint (green). Deflection at the fiberglass spring provides corresponding measurement of the output torque.

to understand the effect of magnitude changes when providing assistance during walking using a hip exoskeleton.

This letter provides three core contributions to the field of assistive lower limb robotics. This letter presents a novel hip exoskeleton (Fig. 1A) utilizing a ball screw driven series elastic actuator (SEA) for power assistance at the hip joint in both hip flexion and extension along the sagittal plane. The device achieves a high fidelity closed loop torque control with a measurement of fiberglass spring deflection. This device presents an excellent test-bed for understanding assistance levels. Secondly, this letter presents a novel controller design that mimics a human biological hip torque profile during the gait cycle. The proposed controller is capable of applying different control parameters such as assistance onset timing, duration, and magnitude with the aid of different mechanical sensors on the device. Thirdly, this letter rigorously tests the design and controller through a ten human subject test to determine the effects of assistance level on energetic cost savings. These results highlight the experimental value of our test-bed system and illustrate that an optimal assistance magnitude indeed exists.

The overall goal of our work is to determine the optimal assistance level applied at the hip joint using a powered exoskeleton during walking. The in depth understanding of relationship between the hip assistance levels and energetic cost savings using an exoskeleton will aid the field to move forward in developing an optimal exoskeleton device. We hypothesize that the increase of exoskeleton assistance provided at the hip joint will off load the work done by the hip flexor/extensor hence, reducing the metabolic cost of walking.

II. Powered Hip Exoskeleton Design

We designed a bilateral hip exoskeleton device (Fig. 1B) to apply torque at the user's hip joint during walking. The overall mass of the device is around 7 kg where the main components of the device are actuators (1.5 kg each), main frame structure (2 kg), orthosis (1.5 kg for both waist band and thigh cuffs), and the on board electronics (0.5 kg). The device is capable of providing a peak torque of 60 Nm and a maximum continuous torque of 30 Nm with an angular velocity up to 180 °/sec. The desired exoskeleton peak and maximum continuous torque parameters were derived using Eq. 1 and Eq. 2 based on the biomechanic data [28]–[30] where $\tau(v)$ is the human biological hip moment over one gait cycle, v is the walking speed, m is the subject's body mass, and n is the number of moment data points over one gait cycle.

$$\tau(v)_{peak} = \frac{m}{2}\left(|\tau_{\min}(v)| + \tau_{\max}(v)\right) \tag{1}$$

$$\tau(v)_{cont} = m\sqrt{\frac{\sum_{i=1}^{n}\tau(v)_i^2}{n}} \tag{2}$$

Using the both equations, our device can support approximately 90% of peak and maximum continuous torque for an average body mass of 70 kg subject walking at 1.2 m/s. The device allows 100° and 30° range of motion in the sagittal plane for maximum hip flexion and extension respectively. Additionally, a passive hinge joint allows for 15° of movement for both hip ab/adduction along the frontal plane. The entire device has three different attachment points to the user: orthotic thigh shell, pelvic band, and shoulder straps. Each attachment point can be adjusted to accommodate different body sizes.

A. Mechatronic Design

The powered bilateral hip exoskeleton consists of two ball screw driven series elastic actuators (SEAs) (Fig. 1C). The motor torque is initially speed reduced with a 2:1 timing belt transmission where the output torque is converted into a linear force with the ball nut travelling along the ball screw shaft with a carbon fiber tube attached to it. The ball screw transmission was chosen because it provides high efficiency and back drivability in a light weight package [31]. The entire actuator rotates along the pivot point located at the motor housing as the actuator extends or retracts. Lastly, the carbon fiber actuator is coupled in series with a fiberglass leaf spring where the deflection of the spring is measured with a set of strain gauges mounted in a form of full Wheatstone bridge. The use of a fiberglass spring enables reduced mass [32]. Each SEA is mounted to a main C-shaped frame made of carbon fiber, which ensures the orientation of the device is upright when the user is fitted. The user interface, which includes the thigh orthosis, the pelvic band, and the polycarbonate back plate, is attached to the main frame. The back plate holds the electronics as well as shoulder straps.

The 200 W brushless DC motor rated at 36 V (EC 30, Maxon Motor) is controlled with a single board computer (myRIO, National Instrument). The myRIO is equipped with a FPGA chip for a closed loop torque control with a PD controller using the spring deflection reading measured with from the strain gauge (Omega Engineering). A servo driver (ESCON 50/5 Module, Maxon Motor) operates in current control mode and uses a Hall

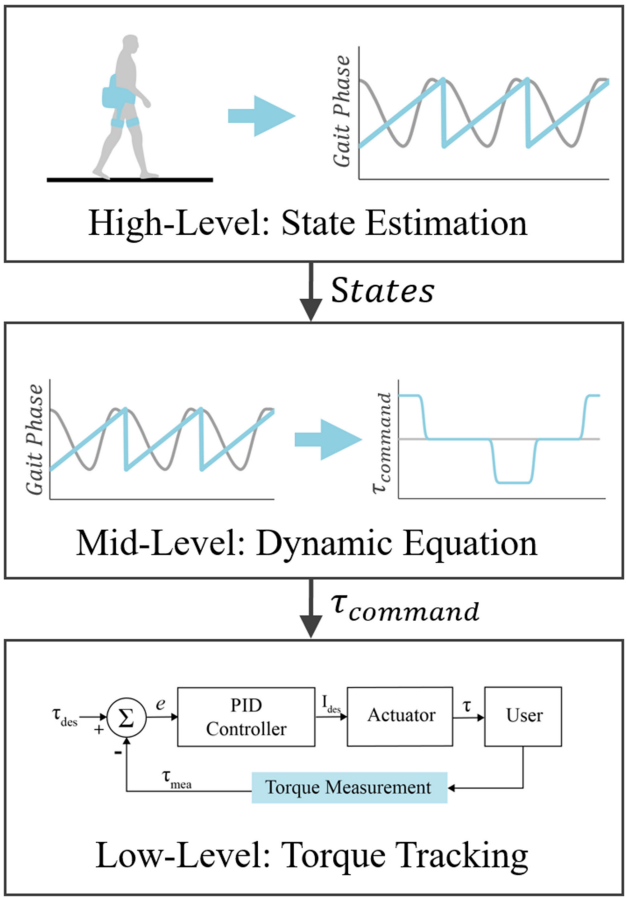

Fig. 2. Control system architecture of the exoskeleton device. On board computer interacts with different mechanical sensors on the device for high level control and commands the desired torque in currents to a servo driver for a low level closed loop torque control.

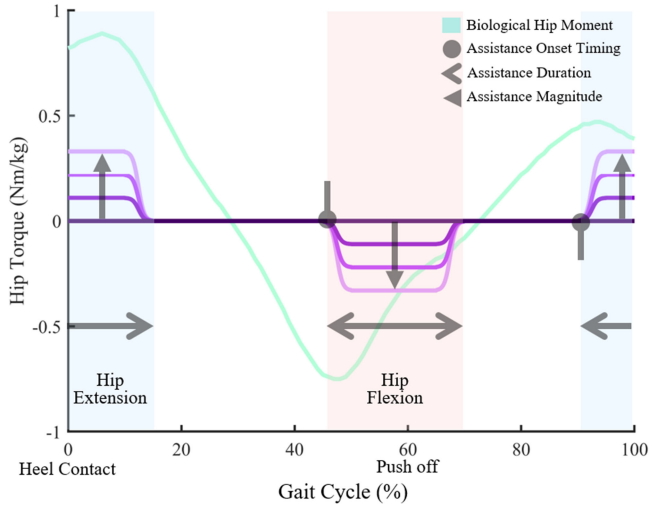

Fig. 3. Example of a commanded torque profile for a biological torque controller. Control profile (shown in purple) emulates a percentage of human biological hip moment (shown in green) over a gait cycle. Hip flexion (red region) and extension (blue region) assistance onset timing, duration, and magnitude (shown with different type of arrows) can be tuned for a desired profile.

effect sensor and an incremental motor shaft encoder for commutation. Both actuators are powered by two 18.5 V lithium polymer batteries (Venom Power) connected in series. A 14-bit absolute magnetic encoder (Orbis, Renishaw) is used to measure the hip joint angle. Three inertial measurement units (IMUs) (Micro USB, Yost Lab) are also mounted on the device. Two IMUs are placed bilaterally on each thigh and one is on the back unit to measure the limb and trunk orientation during walking. Lastly, force sensitive resistors (FSRs) are placed on each heel of the user to detect the heel contact during walking. An additional custom made printed circuit board is used for reading and filtering the analog sensor signals such as strain gauge amplifier for spring measurements. All of the on board mechanical sensor data are collected by myRIO for high and mid-level control such as estimating the gait phase and generating the torque assistance profile.

B. Controller Design

The exoskeleton device control layer is broken down into three tiers for its purpose: high, mid, and low-level layers (Fig. 2). The high-level layer implements an algorithm to estimate the user's state such as gait phase. This aspect is critical as it provides information regarding the timing for power assistance. While it is mainly used for estimating the gait phase in this study, this layer can be enhanced with additional control algorithms such as classifying the user's intent with machine learning techniques. The mid-level layer dictates the device dynamic performance. This layer can implement different dynamic controllers used in the literature such as admittance, position, and myoelectric control [22], [33], [34]. For this study, our exoskeleton incorporates a torque controller where the commanded torque profile is generated with given timing and magnitude parameters with additional user state information computed from the high-level layer. Lastly, the low-level layer ensures that the output torque meets the desired torque by applying a closed loop torque control.

Our biological torque controller mimics the human biological hip moment profile (Fig. 3). Over a gait cycle, the controller can generate a torque assistance for both hip flexion and extension with predefined control parameters. The three key parameters that dictate the assistance profile are onset timing, assistance duration, and assistance magnitude. The onset timing parameter was used with values found from our previous work [27] which was 45% and 90% of the gait cycle for hip flexion and extension respectively (where 0% is defined as heel contact). Assistance duration was optimized with an initial pilot test. Lastly, assistance magnitude can be changed relative to percentage of peak human biological hip moment during the gait cycle [29]. The peak biological hip moment value was normalized to the user's bodyweight to provide appropriate assistance magnitude.

The biological torque controller (Eq. 3) intakes a gait phase percentage, x, as an input and outputs a commanded torque, $f(x)$, where o_f and o_e are flexion and extension onset timing respectively and d is the assistance duration all relative to the gait phase.

$$f(x) = \begin{cases} -g\left(x - o_f\right), & o_f \leq x < \mathrm{mod}\left(\left(o_f + d\right), 100\right) \\ g\left(x - o_e\right), & o_e \leq x < \mathrm{mod}\left(\left(o_e + d\right), 100\right) \\ 0, & \text{otherwise} \end{cases} \tag{3}$$

$g(z)$ represents a function generating a single trapezoidal profile (Eq. 4) with a desired assistance magnitude u, input phase z,

assistance u starting and ending set point s_1 and s_2 respectively, all relative to the gait phase. The assistance magnitude u (Eq. 5) is computed using the desired assistance level a (%) and the peak human biological hip moment, $\tau(v)_{peak}$, calculated from Eq. 1.

$$g(z) = \begin{cases} \frac{uz}{s_1}, & 0 \le z < s_1 \\ u, & s_1 \le z < s_2 \\ -\frac{u(z-s_2)}{d-s_2} + u, & s_2 \le z < d \end{cases} \quad (4)$$

$$u = a\tau(v)_{peak} \quad (5)$$

During the gait cycle where the assistance is not provided, the device is put into zero impedance mode which is simply generating the interaction torque that is measured between the user and the actuator output. Due to the gear reduction stage in the mechanical transmission in the SEA, it exerts non-negligible interaction torque to the user when walking which hinders natural movement. To minimize this resistance, the device outputs an equal amount of torque to allow the user to move the limb freely, hence called zero impedance mode. A video of a subject walking in both assistance and zero impedance mode is included in the supplemental material.

As the biological torque controller is heavily dependent on the gait cycle for generating the correct assistance profile, it is critical to estimate the gait phase accurately in real time. We utilized the FSR sensor to estimate the user's gait phase during walking. While walking, the myRIO stores the timestamp when the heel contact occurs through the FSR sensor readings. From this, a stride time was calculated by taking the time difference between the heel strikes. Using the previous five stride times, we calculated the average stride duration. Finally, the time since the most recent heel contact was divided by this average stride duration in order to compute the current gait phase in percentage [35].

III. Initial Human Characterization

An initial study was conducted to characterize the device performance. During this process, several key factors contributing to the device performance were observed: the device impedance in terms of actuator interaction torque, controller performance in terms of zero impedance mode compensating the interaction torque, and the low-level controller performance regarding torque tracking of the closed loop torque control.

A. Exoskeleton Human Performance Characterization

We conducted a pilot test where three able-bodied subjects (body mass of 71.3 $\pm$ 5.5 kg) walked on a treadmill at 0.4 m/s with the exoskeleton to analyze the controller's capability in compensating the interaction torque during zero impedance mode. During this testing, we collected the user's metabolic cost of walking to observe the zero impedance mode performance in terms of human energetics. The low treadmill speed was mainly due to the limitations of walking with the device powered off. When the device is powered off, the actuator has a certain impedance (interaction torque), mainly from the gear transmission and friction, which impedes the user's hip movement. The treadmill speed was chosen carefully so that the user could still easily walk normally. Overall, the user walked in four different conditions: exoskeleton powered off, actuator off (exoskeleton without the SEA), exoskeleton in zero impedance mode, and no exoskeleton condition. We have added the actuator off condition where the spring linkage was disconnected from the transmission so that the actuator output does not exert any interaction torque to the user. This condition can provide an additional baseline information (along with no exoskeleton condition) to compare the controller performance with the exoskeleton mass added to the user (but not the impedance). The average metabolic costs of walking, after subtracting out the resting metabolic cost, were measured to be 1.92 $\pm$ 0.25 W/kg, 1.33 $\pm$ 0.13 W/kg, 1.59 $\pm$ 0.13 W/kg, and 0.75 $\pm$ 0.04 W/kg for exoskeleton powered off, actuator off, exoskeleton in zero impedance mode, and no exoskeleton condition respectively. It was observed that the powered off condition can increase the net metabolic cost nearly twice compared to the no exoskeleton condition. According to the literature studies, theoretical increase of metabolic cost of walking can be evaluated with the exoskeleton mass added [36], [37]. Since the exoskeleton mass added to the user can be represented as the actuator off condition, metabolic cost result comparison between zero impedance mode and the actuator off condition could validate whether the zero impedance mode can be used as a baseline condition. While the zero impedance mode did not yield the same metabolic cost

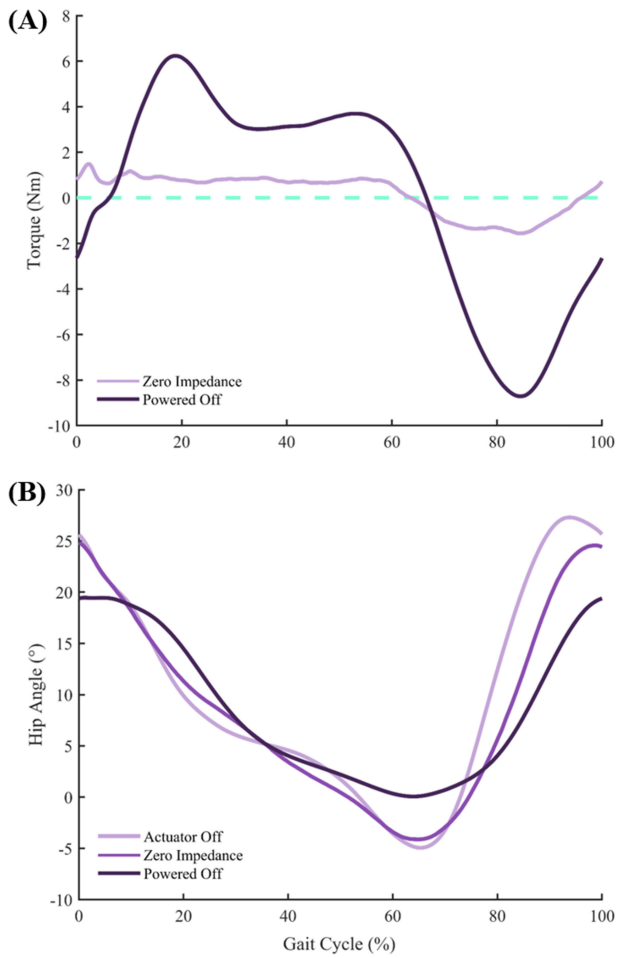

Fig. 4. Initial human characterization results of the exoskeleton device. (A) Actuator interaction torque compensation. When the actuator operates with zero impedance mode, the interaction torque (shown in purple) that is exerted due to mechanical impedance of the transmission in the SEA was greatly reduced compared to the unpowered mode. (B) Hip joint kinematics across different actuator conditions. Actuator off condition is where the spring is disconnected from the output hip joint to allow the user to freely move the hip joint without any impedance.

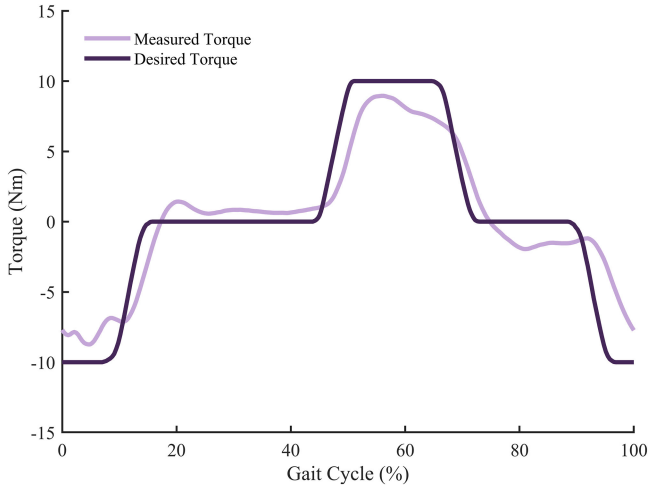

Fig. 5. Torque tracking of the assistance torque profile of the gait cycle. A 10 Nm torque was assisted to the user during walking with predefined control parameters (onset timing and assistance duration). The overall mean RMS error was calculated to be 2.15 Nm over a gait cycle.

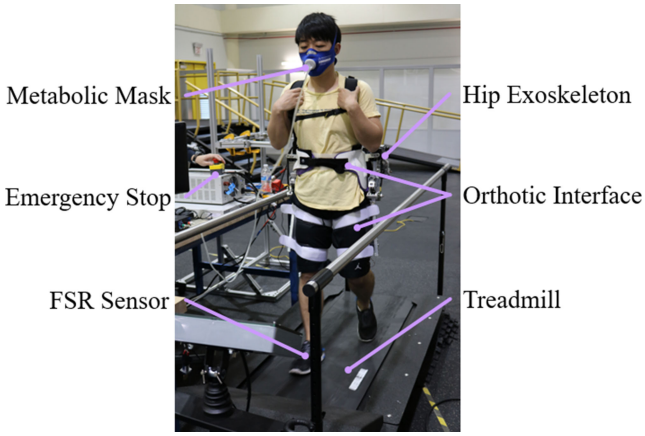

Fig. 6. Experimental setup of the exoskeleton device testing. The user is fitted with a metabolic mask to measure the energy expenditure while wearing the hip exoskeleton.

reduction as the actuator off condition (mainly due to the residual torque in zero impedance mode), it was capable of reducing the metabolic cost vastly and compensated the impedance caused from the actuator. While these metabolic cost measurements cannot be utilized directly in the main experiment mainly due to difference in walking speed, this validation process allowed to quantify the exoskeleton actuator performance in terms of metabolic cost.

The metabolic cost compensation from the zero impedance mode aligned well with the kinetic compensation results (Fig. 4). The RMS interaction torque between the exoskeleton and the human user was reduced from 4.66 Nm to 0.94 Nm using the zero impedance controller during walking (Fig. 4A). During this pilot experiment, more in depth characterization of the actuator behavior was investigated by observing how the interaction torques affect the human gait biomechanics during walking, specifically the hip joint angle (Fig. 4B). The pilot results showed that the actuator output produces non-negligible interaction torque to the user. Moreover, this interaction torque showed that it impedes the user significantly and causes them to reduce the hip joint's range of motion. This was demonstrated in that the peak hip flexion and extension angles were both reduced by 5° each. However, with zero impedance mode, the user's kinematics were closely consistent with the actuator physically disconnected. This illustrates the importance of effective zero impedance mode.

Another preliminary assessment of the device design was to quantify torque tracking of the desired torque with the actual interface torque (Fig. 5). This can be validated by observing the low-level control performance with torque tracking during assistance mode. During the pilot testing, a user was assisted with 10 Nm for both flexion and extension with prechosen controller parameters (onset timing and assistance duration) while walking on a treadmill at 0.4 m/s for 2 minutes. The assistance profile in terms of actual torque measured followed the desired torque correctly validating that the desired torque was assisted. Overall, the RMS error over the 2 minute trial compared to the desired torque profile was 2.15 Nm. A video displaying the low-level torque tracking with hip assistance is included in the supplemental material.

B. *Assistance Duration Optimization Characterization*

A pilot test was conducted to determine the optimal duration of hip flexion and extension for the controller. The subject walked on the treadmill with 0.8 m/s walking speed for six minutes with 26% of the subject's bodyweight for assistance magnitude for both hip flexion and extension. The assistance duration window length was swept from 20% to 35% of the gait cycle with a 5% increment. The metabolic cost reduction for each condition was 6.2% for 20%, 14.6% for 25%, 11.2% for 30%, and 11.0% for 35% all relative to metabolic cost of walking in zero impedance mode. As the 25% window length achieved the highest metabolic cost reduction, the value was used for both hip flexion and extension assistance duration for the main experiment.

IV. Human Subject Testing

A. *Experimental Design*

The study was approved by the Georgia Institute of Technology Institutional Review Board, and informed written consent was obtained for all subjects. Ten healthy subjects (seven males and three females) with an average age of 22.4 ± 2.0 years, body mass of 70.6 ± 8.6 kg, and height of 1.73 ± 0.1 m were recruited. The subjects were asked to walk on the treadmill (TuffTread) for six minutes at 0.8 m/s walking speed in four different assistance conditions where one of them was the zero impedance mode (Fig. 6). The other three assistance conditions are 13%, 26%, and 40% of the peak hip flexion/extension moment based on subject's bodyweight at 0.8 m/s walking speed [29]. The walking speed was set as 0.8 m/s due to device limitation in providing high torque at faster walking speeds. Other control parameters such as onset timing (45% and 90% of flexion and extension) and assistance duration (25% of the gait cycle) were fixed throughout the entire experiment for assistance conditions. During all walking conditions, metabolic cost of walking was measured using an indirect calorimetry system. Before subjects began walking, we measured their resting metabolic rate for 3 minutes while they stood still wearing the exoskeleton. The metabolic cost was calculated using the modified Brockway equation [38] for the last 3 minutes of each six-minute trial to determine the metabolic energy expenditure. Each walking measurement was subtracted with the metabolic cost of a

TABLE I
KINEMATIC AND KINETIC RESULTS ACROSS DIFFERENT EXOSKELETON ASSISTANCE LEVELS

Assistance Level (%)	Joint Kinematic			Joint Torque				
	Peak flexion (°)	Peak extension (°)	Range of motion (°)	Peak flexion torque (Nm)	Peak extension torque (Nm)	RMS flexion torque (Nm)	RMS extension torque (Nm)	Net RMS torque over a gait cycle (Nm)
0	32.07	-5.06	37.13	1.41	0.95	0.76	0.61	0.55
13	33.37	-5.43	38.8	4.82	4.14	3.41	2.31	2.87
26	35.37	-4.24	39.62	8.95	8.73	6.95	6.23	6.04
40	36.33	-4.16	40.5	12.81	13.37	10.24	9.83	8.89

All of the joint kinematic and kinetic results are represented with an averaged value across 10 subjects. Flexion and extension joint torques were decoupled by computing the torque during flexion (45%∼70%) and extension (90%∼15%) region of the gait cycle. For zero impedance mode, flexion and extension torque were computed respect to 0 Nm to calculate the residual interaction torque.

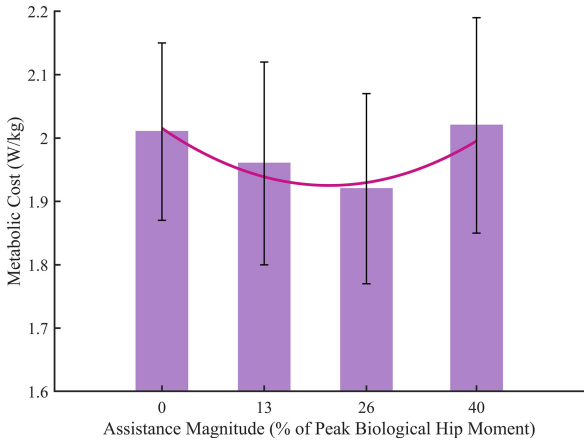

Fig. 7. Metabolic cost result with different assistance magnitude during walking. Generally, increase of assistance magnitude achieved decrease in net metabolic cost of walking except for the highest assistance condition (40% condition) where the metabolic cost increased. The quadratic fit of the metabolic result computed that the maximum metabolic cost can be benefited with 6% reduction from the zero impedance mode with 20% assistance magnitude. Error bar in the graph represents +/− 1 SEM.

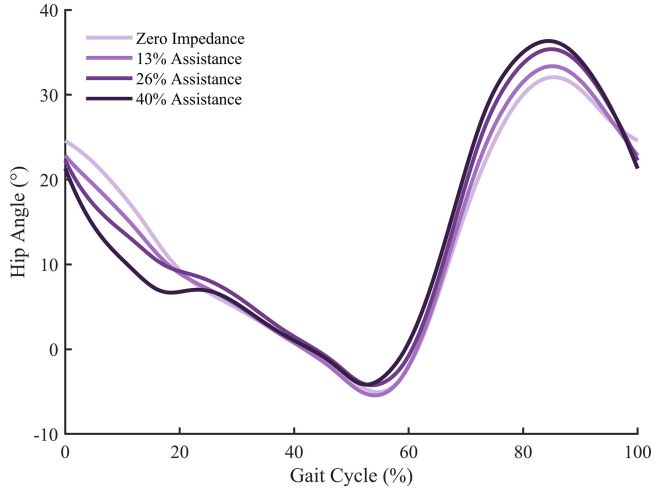

Fig. 8. Average hip kinematics across subjects during different magnitude of assistance levels. Darker shades represent increase of assistance level. With higher assistance magnitude, peak hip flexion angle increased.

resting condition. Additional biomechanic data such as the hip joint torque and angle were measured using the device's SEA and encoder during walking in each condition.

All of the joint kinematic and kinetic results are represented with an averaged value across 10 subjects. Flexion and extension joint torques were decoupled by computing the torque during flexion (45%∼70%) and extension (90%∼15%) region of the gait cycle. For zero impedance mode, flexion and extension torque were computed respect to 0 Nm to calculate the residual interaction torque.

A regression analysis was run to the overall metabolic cost of all subjects across different assist conditions to observe a general trend. Both linear and quadratic fits were run where each coefficient of determination (R^2) was calculated to evaluate the goodness of fit. Furthermore, a pairwise t-test was conducted by calculating the goodness of fit for both linear and quadratic fit to observe if this trend is repeatable across all subjects by setting α to 0.05.

V. RESULTS

Across the different assistance conditions, general trend showed that there was a U-shaped trend where the global optima for the lowest metabolic cost were in between the 13% and 26% conditions (Fig. 7). For the average metabolic cost results, a quadratic and a linear fit had the R^2 value of 0.869 and 9.38×10^{-5} respectively. A pairwise t-test result showed a statistical significance of the R^2 of a quadratic fit to linear fit ($p < 0.01$). Using the quadratic fit to the metabolic cost model, theoretical maximum reduction of metabolic cost was computed to be 6% reduction compared to zero impedance mode. The RMS torque that was applied to the user during the flexion and extension region linearly scaled with different assistance levels while maintaining relatively constant residual interaction torque and showed that similar amount of assistance were provided for both regions during the gait cycle (Table I). Additionally, a post hoc analysis was conducted to compute the continuous torque that was applied to the user over a gait cycle for each assistance levels (normalized by the walking speed) which was 3.59 $\mathrm{Nm/m{\cdot}s^{-1}}$ for 13%, 7.55 $\mathrm{Nm/m{\cdot}s^{-1}}$ for 26%, and 11.11 $\mathrm{Nm/m{\cdot}s^{-1}}$ for 40% respectively. Using the computed torque values, normalized continuous torque over a gait cycle at 20% was found to be 5.62 $\mathrm{Nm/m{\cdot}s^{-1}}$, which is what the study supports as the optimal continuous torque level for exoskeleton design.

Hip joint kinematics changed with varying levels of assistance magnitude (Fig. 8 and Table I). During the first part of stance phase (from 0% to 15% of the gait cycle), there was an excessive hip extension with the increase of assistance magnitude. The average RMS error of hip kinematic deviation in the early stance across subjects was 1.21° for 13%, 2.57° for 26%, and 3.96° for 40% compared to the zero impedance mode. For the remaining early stance (up to 30% of the gait cycle), the hip kinematics returned to the normal hip joint trajectory. In late stance (right before the push off), the hip kinematic started to deviate again where the increase of assistance resulted in higher

hip flexion. Especially when transiting to the mid swing (around 80% of the gait cycle), the peak hip flexion angle increased significantly with higher assistance. The average peak hip flexion across subjects increased 4% for 13%, 10.7% for 26%, and 15% for 40% assistance compared to zero impedance mode where the peak flexion occurred at approximately 85% of the gait cycle. Moreover, the average hip joint range of motion across subjects increased 4.49% for 13%, 6.71% for 26%, and 18.93% for 40% assistance compared to zero impedance mode. The quadratic fit best represented the resulting hip range of motion with different assistance levels ($R^2 = 0.962$).

Additionally, the excessive hip flexion (Especially in the 40% assistance condition) caused the subject to walk in a marching gait pattern. This gait pattern increased the overall stride frequency linearly with the increase of assistance levels. The average stride frequency across subjects was 0.75 stride/sec for zero impedance, 0.78 stride/sec for 13%, 0.81 stride/sec for 26%, and 0.84 stride/sec for 40% assistance. The linear regression showed that the assistance level and stride frequency indeed have a linear relationship ($R^2 = 0.999$). The stride frequency in zero impedance mode correlated well with human biomechanics data with the same walking speed [28]. A video of a subject walking in a marching gait pattern with hip assistance at maximal levels is included in the supplemental material.

VI. Discussion

Overall, our exoskeleton was able to show a positive result in achieving metabolic cost benefits with the increase of assistance level. Our study resulted in a similar metabolic cost reduction (6% when optimized) compared to other recent exoskeleton studies [21], [25], [39]. For example, Seo *et al*. utilized an adaptive oscillator controller that generated a torque profile similar to our biological torque controller and was able to achieve a substantial amount metabolic cost reduction ($\sim$13%) compared to no exoskeleton condition using a lightweight hip exoskeleton [21]. Ding *et al*. was also able to achieve a considerable amount of metabolic cost reduction (between 5.7$\sim$8.5%) with cable driven hip extension assistance compared to unpowered condition [25]. The range of metabolic cost benefit differences across the studies were mainly due to other confounding factors such as the device structure and controller architecture.

While providing hip assistance resulted a metabolic cost reduction, our initial hypothesis was rejected in that increase of assistance level did not yield higher metabolic cost reduction. The resulting U-shaped trend of metabolic cost provides an important information that there is an optimum for exoskeleton assistance to attain the best metabolic cost benefits. Our study resulted in a similar quadratic trend as the relevant literature study using the ankle exoskeleton [40]. While the study may not directly correlate with our work (as the ankle joint has different musculotendon structure than the hip joint), the general results aligned that excessive assistance at the joint may penalize both mechanically and biologically. Similar to the literature studies on assistance timing study [26], [27], the assistance magnitude should be optimized for best energetic savings rather than just being set as high as physically possible. Moreover, while it was outside the scope of this study, a possible future work can observe the energetic effect of hip assistance when the magnitude ratio of extension to flexion varies to fully optimize the hip assistance levels.

Mainly we observed that larger assistance magnitudes biased the hip kinematics in the flexion direction during swing phase (Fig. 8). This excessive hip flexion induced a marching gait which increased the user's stride frequencies. Generally, increased stride frequencies in marching gait will direct the user to take shorter steps. Considering the stance phase as an inverted pendulum motion, positive work at the center of mass is required to restore the energy lost during the collision occurring at the heel contact [41], [42]. As increase in the exoskeleton assistance decreases the user's step length, overall negative work done through the collision gets reduced hence, higher metabolic cost reduction.

On the other hand, the increase of stride frequencies in higher assistance levels penalize the net metabolic cost. Along with stride frequencies, results showed that the hip joint range of motion exhibited quadratic growth with increase of assistance levels which will force the subject to have a faster leg swing. Literature studies have shown that increase in the stride frequencies correlates with faster swinging leg motion where muscle fibers are required to produce larger forces at short durations. Overall, this will result in a higher metabolic cost due to the low economy muscle generating the required force over short time [43], [44]. Two main factors relating to increase in assistance, stride frequencies and collision time, direct the metabolic cost in an opposite direction which explains the reason for achieving a general U-shaped trend for the resulting metabolic cost where ideally the cross over point of two factors is the optimal assistance magnitude that attains highest metabolic cost reduction.

Our findings in regard to optimal assistance levels provide valuable information about the exoskeleton design. For example, computed continuous torque to achieve the best metabolic cost benefits can help future exoskeleton designers to optimize the actuator specification. Furthermore, the non-negligible energy loss through the user interface should be investigated more as it may have affected the result. The hip kinematic deviation occurring at the early stance phase occurred due to the soft tissue of the limb segment. This dampening effect in the limb limits the exoskeleton by delaying the assistance applied at the skeletal structure. Lastly, further exploration in the interaction between control parameters such as integrating the human-in-the-loop optimization may be useful [18], [24]. This approach can improve the exoskeleton controller by having the control parameter scale to the user's state such as the user's stride frequencies. Through this, the dynamic controller may be able to accommodate the assistance in a stride by stride basis.

VII. Conclusion

Our powered hip exoskeleton showed that the metabolic cost reduction does not correlate linearly with assistance magnitude. The underlying biomechanical effects in the user during exoskeleton assistance resulted in a U-shaped trend in the metabolic cost. The exhibited exoskeleton behavior illustrated the importance of understanding human robot interaction. Moreover, as our result showed that additional levels of support are undesirable, there are clear ramifications for system design. Future exoskeleton designers can utilize our findings to further investigate to optimize the mechatronic design for a more robust and versatile exoskeleton. Lastly, implementation of an integrated controller capable of scaling parameters dynamically may aid the exoskeleton technology to be translated to more realistic settings such as outdoor environments.

ACKNOWLEDGMENT

The authors would like to thank Dr. G. Kogler for his insights in designing the orthotic interface, C. Kilpatrick and S. E. Lee for their help in fabricating the interface, and J. Li and R. Hong for data collection. The authors would also like to thank C. Bivens and M. Mayo at Georgia Tech Research Institute for their contributions.

REFERENCES

[1] A. J. Young and D. P. Ferris, "State of the art and future directions for lower limb robotic exoskeletons," *IEEE Trans. Neural Syst. Rehabil. Eng.*, vol. 25, no. 2, pp. 171–182, Feb. 2017.

[2] T. Yan, M. Cempini, C. M. Oddo, and N. Vitiello, "Review of assistive strategies in powered lower-limb orthoses and exoskeletons," *Robot. Auton. Syst.*, vol. 64, pp. 120–136, 2015.

[3] W. Huo, S. Mohammed, J. C. Moreno, and Y. Amirat, "Lower limb wearable robots for assistance and rehabilitation: A state of the art," *IEEE Syst. J.*, vol. 10, no. 3, pp. 1068–1081, Sep. 2016.

[4] H. Hodson, "Robotic suit gives shipyard workers super strength," New Scientist, Aug. 2014. [Online]. Available: https://www.newscientist.com/article/mg22329803-900-robotic-suit-gives-shipyard-workers-super-strength/

[5] H. Yu, I. S. Choi, K.-L. Han, J. Y. Choi, G. Chung, and J. Suh, "Development of a upper-limb exoskeleton robot for refractory construction," *Control Eng. Pract.*, vol. 72, pp. 104–113, 2018.

[6] A. B. Zoss, H. Kazerooni, and A. Chu, "Biomechanical design of the Berkeley lower extremity exoskeleton (BLEEX)," *IEEE/ASME Trans. Mechatronics*, vol. 11, no. 2, pp. 128–138, Apr. 2006.

[7] F. A. Panizzolo *et al.*, "A biologically-inspired multi-joint soft exosuit that can reduce the energy cost of loaded walking," *J. NeuroEng. Rehabil.*, vol. 13, no. 1, p. 43, 2016.

[8] R. J. Farris, H. A. Quintero, S. A. Murray, K. H. Ha, C. Hartigan, and M. Goldfarb, "A preliminary assessment of legged mobility provided by a lower limb exoskeleton for persons with paraplegia," *IEEE Trans. Neural Syst. Rehabil. Eng.*, vol. 22, no. 3, pp. 482–490, May 2014.

[9] G. Zeilig, H. Weingarden, M. Zwecker, I. Dudkiewicz, A. Bloch, and A. Esquenazi, "Safety and tolerance of the ReWalk exoskeleton suit for ambulation by people with complete spinal cord injury: A pilot study," *J. Spinal Cord Med.*, vol. 35, no. 2, pp. 101–96, 2012.

[10] L. N. Awad *et al.*, "A soft robotic exosuit improves walking in patients after stroke," *Sci. Transl. Med.*, vol. 9, no. 400, 2017, Art. no. eaai9084, doi: 10.1126/scitranslmed.aai9084.

[11] M. Sczesny-Kaiser *et al.*, "Neurorehabilitation in chronic paraplegic patients with the HAL exoskeleton–preliminary electrophysiological and fMRI data of a pilot study," in *Converging Clinical and Engineering Research on Neurorehabilitation*, J. L. Pons, D. Torricelli, and M. Pajaro, Eds., Berlin, Germany: Springer-Verlag, 2013, pp. 611–615.

[12] S. A. Kolakowsky-Hayner, J. Crew, S. Moran, and A. Shah, "Safety and feasibility of using the EksoTM bionic exoskeleton to aid ambulation after spinal cord injury," *J. Spine*, vol. 2, no. 1, pp. 1–8, 2013.

[13] M. Cenciarini and A. M. Dollar, "Biomechanical considerations in the design of lower limb exoskeletons," in *Proc. IEEE Int. Conf. Rehabil. Robot.*, 2011, pp. 1–6.

[14] L. Mooney, E. Rouse, and H. Herr, "Autonomous exoskeleton reduces metabolic cost of human walking during load carriage," *J. NeuroEng. Rehabil.*, vol. 11, no. 1, 2014, Art. no. 80.

[15] A. Asbeck, S. De Rossi, K. Holt, and C. Walsh, "A biologically inspired soft exosuit for walking assistance," *Int. J. Robot. Res.*, vol. 34, no. 6, pp. 744–762, 2015.

[16] K. A. Witte, J. Zhang, R. W. Jackson, and S. H. Collins, "Design of two lightweight, high-bandwidth torque-controlled ankle exoskeletons," in *Proc. IEEE Int. Conf. Robot. Automat.*, 2015, pp. 1223–1228.

[17] F. Giovacchini *et al.*, "A light-weight active orthosis for hip movement assistance," *Robot. Auton. Syst.*, vol. 73, pp. 123–134, 2015.

[18] J. Zhang *et al.*, "Human-in-the-loop optimization of exoskeleton assistance during walking," *Science*, vol. 356, no. 6344, p. 1280, 2017, doi: 10.1126/science.aal5054.

[19] G. S. Sawicki, C. L. Lewis, and D. P. Ferris, "It pays to have a spring in your step," *Exercise Sport Sci. Rev.*, vol. 37, no. 3, p. 130, 2009.

[20] B. R. Umberger and J. Rubenson, "Understanding muscle energetics in locomotion: New modeling and experimental approaches," *Exercise Sport Sci. Rev.*, vol. 39, no. 2, pp. 59–67, 2011.

[21] K. Seo, J. Lee, Y. Lee, T. Ha, and Y. Shim, "Fully autonomous hip exoskeleton saves metabolic cost of walking," in *Proc. IEEE Int. Conf. Robot. Automat.*, 2016, pp. 4628–4635.

[22] T. Zhang, M. Tran, and H. Huang, "Design and experimental verification of hip exoskeleton with balance capacities for walking assistance," *IEEE/ASME Trans. Mechatronics*, vol. 23, no. 1, pp. 274–285, Feb. 2018.

[23] Y. Kusuda, "In quest of mobility–Honda to develop walking assist devices," *Ind. Robot: Int. J.*, vol. 36, no. 6, pp. 537–539, 2009.

[24] Y. Ding, M. Kim, S. Kuindersma, and C. J. Walsh, "Human-in-the-loop optimization of hip assistance with a soft exosuit during walking," *Sci. Robot.*, vol. 3, no. 15, 2018, Art. no. eaar5438, doi: 10.1126/scirobotics.aar5438.

[25] Y. Ding *et al.*, "Effect of timing of hip extension assistance during loaded walking with a soft exosuit," *J. NeuroEng. Rehabil.*, vol. 13, no. 1, 2016, Art. no. 87.

[26] P. Malcolm, W. Derave, S. Galle, and D. De Clercq, "A simple exoskeleton that assists plantarflexion can reduce the metabolic cost of human walking," *PLOS ONE*, vol. 8, no. 2, 2013, Art. no. e56137.

[27] A. J. Young, J. Foss, H. Gannon, and D. P. Ferris, "Influence of power delivery timing on the energetics and biomechanics of humans wearing a hip exoskeleton," *Frontiers Bioeng. Biotechnol.*, vol. 5, p. 4, 2017.

[28] G. Bovi, M. Rabuffetti, P. Mazzoleni, and M. Ferrarin, "A multiple-task gait analysis approach: Kinematic, kinetic, and EMG reference data for healthy young and adult subjects," *Gait Posture*, vol. 33, no. 1, pp. 6–13, Jan 2011.

[29] K. E. Zelik and A. D. Kuo, "Human walking isn't all hard work: Evidence of soft tissue contributions to energy dissipation and return," *J. Exp. Biol.*, vol. 213, no. 24, pp. 4257–4264, 2010.

[30] D. Winter, J. Eng, and M. Ischac, "Three-dimensional moments, powers and work in normal gait: Implications for clinical assessments," in *Human Motion Analysis: Current Applications and Future Directions*, G. Harris and S. PA, Eds., New York, NY, USA: IEEE Press, 1996.

[31] C. Knabe *et al.*, "Design of a Series Elastic Humanoid for the DARPA Robotics Challenge," in *Proc. IEEE-RAS 15th Int. Conf. Humanoid Robots (Humanoids)*, pp. 738–743, 2015.

[32] M. K. Shepherd and E. J. Rouse, "Design and validation of a torque-controllable knee exoskeleton for sit-to-stand assistance," *IEEE-ASME Trans. Mechatronics*, vol. 22, no. 4, pp. 1695–1704, Aug. 2017.

[33] A. J. Young, H. Gannon, and D. P. Ferris, "A biomechanical comparison of proportional electromyography control to biological torque control using a powered hip exoskeleton," *Frontiers Bioeng. Biotechnol.*, vol. 5, 2017, Art. no. 37, doi: 10.3389/fbioe.2017.00037.

[34] H. Kazerooni, R. Steger, and L. Huang, "Hybrid control of the Berkeley lower extremity exoskeleton (BLEEX)," *Int. J. Robot. Res.*, vol. 25, no. 5/6, pp. 561–573, 2006.

[35] C. L. Lewis and D. P. Ferris, "Invariant hip moment pattern while walking with a robotic hip exoskeleton," *J. Biomech.*, vol. 44, no. 5, pp. 789–793, 2011.

[36] K. B. Pandolf, B. Givoni, and R. F. Goldman, "Predicting energy-expenditure with loads while standing or walking very slowly," *J. Appl. Physiol.*, vol. 43, no. 4, pp. 577–581, 1977.

[37] T. M. Griffin, T. J. Roberts, and R. Kram, "Metabolic cost of generating muscular force in human walking: Insights from load-carrying and speed experiments," *J. Appl. Physiol.*, vol. 95, no. 1, pp. 172–183, 2003.

[38] J. Brockway, "Derivation of formulae used to calculate energy expenditure in man," *Human Nutrition Clin. Nutrition*, vol. 41, no. 6, pp. 463–471, 1987.

[39] R. Ronsse *et al.*, "Oscillator-based assistance of cyclical movements: Model-based and model-free approaches," *Med. Biol. Eng. Comput.*, vol. 49, no. 10, pp. 1173–1185, 2011.

[40] S. H. Collins, M. B. Wiggin, and G. S. Sawicki, "Reducing the energy cost of human walking using an unpowered exoskeleton," *Nature*, vol. 522, pp. 212–215, 2015.

[41] J. M. Donelan, R. Kram, and A. D. Kuo, "Mechanical work for step-to-step transitions is a major determinant of the metabolic cost of human walking," *J. Exp. Biol.*, vol. 205, no. 23, pp. 3717–3727, Dec. 2002.

[42] G. A. Cavagna and R. Margaria, "Mechanics of walking," *J Appl. Physiol.*, vol. 21, no. 1, pp. 271–278, Jan. 1966.

[43] A. D. Kuo, "A simple model of bipedal walking predicts the preferred speed-step length relationships," *J. Biomech. Eng.*, vol. 123, no. 3, pp. 264–269, Jun. 2001.

[44] J. Doke, J. M. Donelan, and A. D. Kuo, "Mechanics and energetics of swinging the human leg," *J. Exp. Biol.*, vol. 208, no. 3, pp. 439–445, 2005, doi: 10.1242/jeb.01408.